JOURNAL OF NEUROTRAUMA 37:1954–1962 (September 15, 2020)

DOI: 10.1089/neu.2019.6974

Original Articles

Analysis of N- and O-Linked Glycosylation: Differential Glycosylation after Rat Spinal Cord Injury

Wupu Osimanjiang,[1] Kelly C. Santos Roballo,[1] Brenda D. Houck,[1] Mai Ito,[2] Aristotelis Antonopoulos,[2] Anne Dell,[2] Stuart M. Haslam,[2] and Jared S. Bushman[1]

Abstract

Glycosylation is a fundamental cellular process that has a dramatic impact on the functionality of glycoconjugates such as proteins or lipids and mediates many different biological interactions including cell migration, cellular signaling, and synaptic interactions in the nervous system. In spinal cord injury (SCI), all of these cellular processes are altered, but the potential contributions of glycosylation changes to these alterations has not been thoroughly investigated.

We studied the glycosylation of injured spinal cord tissue from rats that received a contusion SCI. The N- and O-linked glycosylation was assessed at 3 and 14 days post-injury (DPI), and compared with uninjured control and time-matched sham spinal tissue. Matrix-assisted laser desorption ionization time-of-flight mass spectrometry (MALDI-TOF MS) and tandem MS (MS/MS) were performed to analyze carbohydrate structures. Results revealed diverse and abundant glycosylation in all groups, with some carbohydrate structures differentially produced in SCI animals compared with uninjured controls and shams. One such change occurred in the abundance of the Sda structure, Neu5Ac-α-(2,3)-[GalNAc-β-(1,4)-]Gal-β-(1,4)-GlcNAc, which was increased in SCI samples compared with shams and non-injured controls. Immunohistochemistry (IHC) and western blot were performed on SCI and sham samples using the CT1 antibody, which recognizes the terminal trisaccharide of Sda with high specificity. Both of these metrics confirmed elevated Sda structure in SCI tissue, where IHC further showed that Sda is expressed mainly by microglia. The results of these studies suggest that SCI causes a significant alteration in N- and O-linked glycosylation.

Keywords: carbohydrates; CT1 antibody; glycosylation; Sda; spinal cord injury

Introduction

Spinal cord injury (SCI) is a devastating neurological disorder that affects thousands of people each year.[1] The most common causes of SCIs are, in order, contusion, transection, and compression.[2] A series of adaptive and maladaptive responses follow SCI and include cellular apoptosis, vasculature changes, ischemia, edema, and inflammation.[3] A glial scar is formed after SCI at the injured area by accumulated reactive astrocytes and microglial cells.[4] Although the glial scar suppresses progression of secondary damage after initial insult, it forms an inhibitory environment for axonal regeneration by increasing the production of chondroitin sulfate proteoglycans (CSPGs) and other inhibitory molecules.[4,5] Thus, gaining a complete understanding of the cellular and molecular changes occurring after SCI is essential for the development of effective therapeutic strategies.

Carbohydrates are one of the four main classes of biological molecules with diverse and complex structures in living organisms.[6,7] Carbohydrates can exist as independent molecules but are often attached to proteins and lipids.[6] Carbohydrates, as components of glycoproteins, proteoglycans, and glycolipids, play essential roles in protein folding, cellular recognition, cellular adhesion, cell migration, protection, metabolism, and development.[6,8–10] Glycosylation is ubiquitously present in every part of the body including the nervous system and plays important roles in development, as well as IN functionality of the developed nervous system.[11] Glycosylation mediates axonal glycoprotein trafficking, controls myelination, guides axonal growth, and influences regeneration.[12,13] The knock-out of *Srd5a3*, an important gene for N-glycosylation, in mouse cerebellum causes abnormal granule cell development, impaired neurite growth and axonal guidance, and results in coordination defects.[14] The knock-out of *ogt*, a gene for O-GlcNAc transferase enzyme, which is important for initiation of O-GlcNAc glycosylation, leads to progressive nerve degeneration, increased anxiety, impaired memory, upregulated gliosis, and increased neuroinflammation.[15]

Glycosylation is altered under diseased conditions and these alterations may affect recovery.[11,16,17] Alterations of glycosylation

[1]School of Pharmacy, University of Wyoming, Laramie, Wyoming, USA.
[2]Department of Life Sciences, Imperial College London, London, United Kingdom.

of peroxisome proliferator-activated receptor γ (PPARγ) attenuate inflammatory activation of microglia.[18] Sialylation and fucosylation of N-linked and O-linked polysaccharides are altered in brain cancer, and these differences play critical roles in the progression of the cancer.[19] CSPGs are overexpressed in injured spinal cords and inhibit axonal regeneration.[20] Lewis^x Gal-β-(1,4)-[Fuc-α-(1,3)]-GlcNAc is highly expressed in the developing central nervous system (CNS) and plays critical roles in intercellular recognition, cell differentiation, and cell adhesion, as well as neurite outgrowth.[21–25] Polysialic acid is a large extracellular polysaccharide that promotes axonal regeneration after injury.[26–28] Gangliosides, which are glycolipids present in neuronal membranes, are receptors for myelin-associated glycoprotein (MAG) and support axon stability, contribute to axon myelin interaction, and inhibit axon outgrowth after injury.[29]

Although glycosylation is ubiquitously present in the spinal cord and plays critical roles, the glycome within the spinal cord remains largely unknown.[30] Therefore, identification of differentially produced carbohydrates is crucial for better understanding of the injury process and therapeutic development for SCI. In this study, we performed carbohydrate structural analysis on spinal cord samples from both injured and non-injured rats to determine the structures of carbohydrates generated by N- and O-linked glycosylation and to identify differential glycosylation structures after SCI. This investigation focused on N- and O-linked glycosylation analyzed at 3 and 14 days post-injury (DPI). We observed that spinal cords produce a diverse and abundant array of carbohydrates and that the glycosylation profile changes in the injured spinal cord. We focused our investigation on one of the differentially expressed carbohydrates, Sda, Neu5Ac-α-(2,3)-[GalNAc-β-(1,4)-]Gal-β-(1,4)-GlcNAc. Sda was initially characterized as a blood group structure[31] and we found it to be highly upregulated after SCI. Analysis of expression of Sda showed that microglia within the injury site are the main cell type expressing Sda.

Methods

Animal care

All animals were acquired, cared for, and used in accordance with the National Institutes of Health (NIH) Guide for the Care and Use of Laboratory Animals and followed protocols approved by Institutional Animal Care and Use (IACUC) at University of Wyoming. Rats were placed in animal rooms with a temperature range of 22–24°C, stable humidity, a 12-h day-night cycle, and free access to rodent laboratory food and water. Animals were housed in individual cages for the duration of the study.

Spinal cord injury

Adult male Sprague-Dawley rats were assigned randomly into one of five groups: non-injured control (3 animals), sham or SCI 3 DPI (6 animals per group), or sham or SCI 14 DPI (14 animals per group). SCI surgical procedures were performed as previously described.[32] Briefly, rats were anesthetized by 2% isoflurane inhalation, and the T10 vertebral area was shaved and sterilized using iodine and isopropyl alcohol. Skin was incised, muscles around the T10 vertebra were cleared, and a partial laminectomy was performed at T10. The spine was suspended via clamps near the exposed spinal cord, to ensure the exposed spinal cord was parallel to the horizontal plane of the surgery table. SCI was induced using an NYU Impactor, by dropping a 10-g, 1.1-mm diameter rod onto the exposed spinal cord from a 25-mm height. Musculature and skin were sutured using 6-0 sutures. After surgery, animals received buprenorphine (NDC 42023-179-05, Par Pharmaceutical, Chestnut Ridge, NY, USA, 0.05 mg/kg) twice daily for 3 days, and baytril (cat. no. 101-5977, Bayer Healthcare, LLC, 5 mg/kg) once daily for 7 days. Bladders were expressed twice daily until recovery of bladder function was observed.

Behavioral assessment

The Basso, Beattie, Bresnahan (BBB) scale was used for functional evaluation of recovery as previously described.[32] Briefly, each rat was placed in a circular plastic enclosure and observed by two independent investigators. Each rat was scored during a 4-min session and the observers' scores were averaged to obtain the animal's score at every time-point.

Tissue harvesting and glycomic analysis

At end-points, animals (3 animals per group) were anesthetized with inhalation of 2% isoflurane with pure oxygen. Animals were perfused with saline and T10 spinal cord tissue was harvested and snap frozen in liquid nitrogen.

Spinal cord samples were treated as described previously.[33] Briefly, each spinal cord sample was subjected to sonication in the presence of 3-[(3-cholamidopropyl) dimethylammonio]-1-propanesulfonate hydrate (detergent CHAPS), reduction in 4 M guanidine-HCl (Pierce), carboxymethylation, and trypsin digestion. The digested glycoproteins were then purified by hydrophilic-lipophilic balance (HLB) plus C_{18}-Sep-Pak (cat. no. 186000132, Waters Corp., Hertfordshire, UK). Products from N-linked glycosylation were released by peptide *N*-glycosidase F (E.C. 3.5.1.52, Roche Applied Science) digestion, whereas products from O-linked glycosylation were released by reductive elimination. Released products from N- and O-linked glycosylation were permethylated using the sodium hydroxide procedure and purified by classic C_{18}-Sep-Pak (cat. no. WAT051910, Waters Corp.).

Mass spectrometry (MS) and tandem MS (MS/MS) data were acquired using a 4800 MALDI-TOF/TOF (matrix-assisted laser desorption ionization time-of-flight/time-of-flight) mass spectrometer (Applied Biosystems, Darmstadt, Germany). Permethylated samples were dissolved in 10 μL of methanol and 1 μL of dissolved sample was pre-mixed with 1 μL of matrix (10 mg/mL 3,4-diaminobenzophenone in 75% [v/v] aqueous acetonitrile), spotted onto a target plate, and dried under vacuum. For the MS/MS studies, the collision energy was set to 1 kV, and argon was used as collision gas. The 4700-calibration standard kit, calmix (Applied Biosystems), was used as the external calibrant for the MS mode, and [Glu1] fibrinopeptide B human (Sigma) was used as an external calibrant for the MS/MS mode.

The MS and MS/MS data were processed using Data Explorer 4.9 software (Applied Biosystems). The processed spectra were subjected to manual assignment and annotation with the aid of a glycobioinformatics tool, GlycoWorkBench.[34] The proposed assignments were based on ^{12}C isotopic composition together with knowledge of the biosynthetic pathways. The proposed structures were then confirmed by data obtained from MS/MS experiments.

Immunohistochemistry

SCI experiments matching with those performed for glycosylation structure analysis were duplicated on additional animals for immunohistochemistry (IHC). At end-point, 3 DPI animals and 14 DPI animals were euthanized via perfusion with 4% paraformaldehyde (PFA) in phosphate-buffered saline (PBS; 137 mM NaCl, 2.7 mM KCl, 10 mM Na2HPO4, and 1.8 mM KH2PO4; PH 7.1 $\pm$ 0.1, cat. no. 14200075, Life Technologies). Samples were placed in optimal cutting temperature (OCT) compound (cat. no. 625501-01, Sakura Finetek USA, Inc.) and 20-μm sections were sliced using a cryostat (CM3050 S, Leica Biosystems).

CT1 hybridoma cells were generously provided by Dr. Ramiro Alberio of the University of Nottingham. Hybridoma cells were cultured in Dulbecco's Modified Eagle Medium/Nutrient Mixture F-12 (DMEM/F12; cat. no. 11330032, Gibco Life Technologies) supplemented with 10% fetal bovine serum (FBS; cat. no. 16140071, Gibco) and 5 μg/mL of Baytril for 2–3 days in 5% CO_2 at 37°C. Cells were centrifuged at 300*g* (gravitational force) for 5 min, then supernatant was used to isolate antibody via affinity chromatography using HiTrap IgM Purification HP column (cat. no. 17511001, GE Healthcare Life Sciences).

Fixed sections of spinal cord tissue were washed with PBS 3 times for 5 min each, and blocked using blocking buffer (10% bovine serum albumin [BSA], 1% normal goat serum, 0.3% Triton X-100 in PBS) for 1 h. Sections then were incubated with primary antibodies diluted in dilution buffer (1% BSA, 0.1% normal goat serum, 0.3% Triton X-100 in PBS) at 4°C overnight, washed 3 times for 5 min each, and incubated with secondary antibodies in dilution buffer for 2 h. Sections next were washed 3 times for 5 min each, then stained with 4',6-diamidino-2-phenylindole (DAPI; diluted 1:1000 in PBS, 1 μg/mL, cat. no. 62248, ThermoFisher Scientific) for 7 min. After this washing and staining, slides were covered with mounting media and cover-slipped (cat. no. F6182, Sigma).

To stain Sda structure, CT1 antibody (2 μg/mL, mouse immunoglobulin M [IgM]) was used, followed by FITC conjugated anti-mouse IgM antibody (1:400, 5 μg/mL, cat. no. AP128F, Millipore).

To stain microglial cells, anti-ionized calcium-binding adapter molecule 1 (Iba1) antibody (1:500, 1.12 μg/mL, rabbit IgG, cat. no. NBP2-19019, Novus Biologicals) was used, followed by TRITC conjugated anti-rabbit IgG antibody (1:400, 13.25 μg/mL, cat. no. T6778, Sigma Aldrich) or Alexa Flour® 405 conjugated anti-rabbit IgG antibody (1:400, 5 μg/mL, cat. no. ab175655, abcam).

To stain astrocytes, anti-glial fibrillary acidic protein (GFAP) antibody (1:500, 2 μg/mL, chicken IgY, cat. no. AB5541, Millipore) was used, followed by Alexa Flour® 555 conjugated goat anti-chicken IgY antibody (1:400, 5 μg/mL, cat. no. A21437, ThermoFisher Scientific).

To stain CD8 T cells, anti-CD8 antibody (1:100, 2 μg/mL, mouse IgG, cat. no. sc-1177, Santa Cruz) was used, followed by Alexa Flour® 555 conjugated anti-mouse IgG (1:400, 5 μg/mL, cat. no. A21127, ThermoFisher Scientific).

Sections were imaged on a confocal microscope (Zeiss) and Image J software (NIH) was used to measure CT1 fluorescent intensities. Six sections were averaged to represent each animal, with 6 animals per group in CT1 fluorescent intensities. Bright field images were taken using transmitted light detector (TPMT) under confocal microscope (Zeiss).

Western blot

Spinal cord samples from sham and SCI animals at 14 DPI (5 animals per group) were harvested and tissues were snap frozen in liquid nitrogen. Samples were homogenized and total proteins were extracted as previously described.[35] Protein concentrations were measured via absorbance at 280-nm wavelength and using a standard curve to extrapolate the concentration using Nanodrop (Thermofisher), then relative concentration of protein in each sample was readjusted using band intensities of β-actin with Image J software.

The samples (13 μg/lane) were separated using sodium dodecyl sulphate-polyacrylamide gel electrophoresis (SDS-PAGE) and transferred to nitrocellulose membranes (cat. no. 1620112, Bio-Rad Laboratories, Inc.) as previously described.[36] The membrane was probed with CT1 antibody (2 ug/mL), anti-β-actin antibody (1:5000, 0.42 μg/mL, cat. no. A1978, Sigma, mouse IgG). Secondary antibodies were peroxidase-labeled anti-mouse IgM secondary antibody (1:10,000, 0.08 ug/mL, cat. no. 31440, ThermoFisher) and peroxidase-labeled anti-mouse IgG secondary antibody (1:3000, 0.33 ug/mL, cat. no. 61-6520, ThermoFisher). Blots were developed with chemiluminescent peroxidase substrate (cat. no. CPSOC, Sigma) and visualized on an iBright FL1000 Imager (cat. no. A32748, Invitrgen). Western blot band intensities were measured using Image J software (NIH). An average of 5 animals were represented for each group. Relative expression of Sda structure was measured by CT1 band intensities divided by β-actin band intensities.

Statistical analysis

The statistical analysis was performed using Microsoft Excel and GraphPad Prism 6 (GraphPad Software, Inc., San Diego, CA, USA). Single-factor analysis of variance (ANOVA) was performed for statistical significance. $P \leq 0.05$ was considered as significant difference. Repeated measures ANOVA was performed for the BBB behavioral test.

Results

Spinal cord injuries were generated

The experimental outline is shown in Figure 1. Contusion SCI was performed at T10 using a 10-g rod dropped from a 25-mm height. BBB scores were measured on animals before surgery and 1, 7, and 13 DPI (Fig. 2A). BBB scores fell to 0.6 at 1 DPI for SCI animals and gradually increased up to 9 at 13 DPI. This level of functional impairment and alteration to spinal tissue from this contusion is consistent with previous reports.[32,37] Sham animals remained at a BBB score of 21.

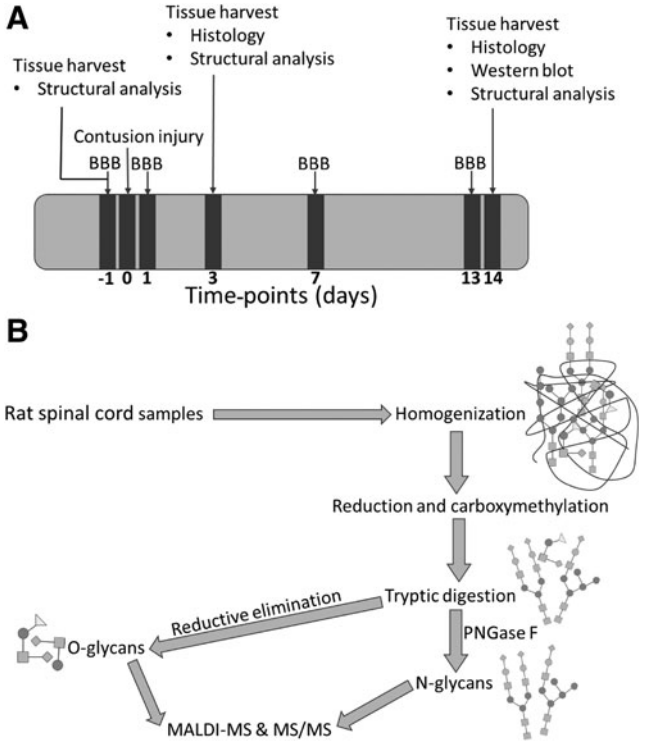

FIG. 1. Time-points of experimental procedures and workflow of carbohydrate structural analysis. **(A)** Timeline of experimental procedures for tissue harvest, tissue analysis, SCI, and functional analysis. **(B)** Workflow of N- and O-linked glycosylation structural analysis from SCI, sham, and control spinal tissue. BBB, Basso, Beattie, Bresnahan scale score; MALDI MS, matrix-assisted laser desorption ionization mass spectrometry; SCI, spinal cord injury.

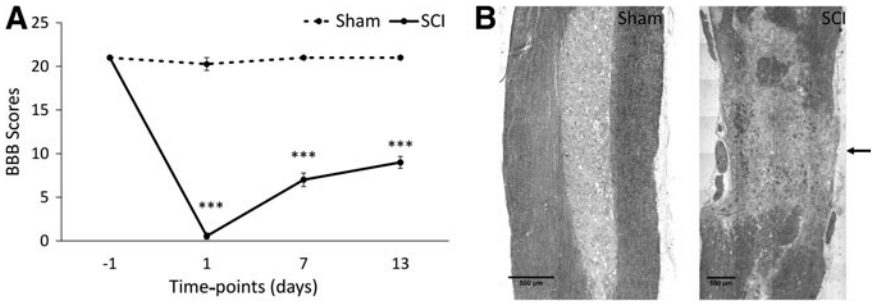

FIG. 2. Functional outcome and characteristics of spinal tissue after contusion injury. **(A)** Level of functional impairment caused by the SCI as assessed by BBB scale scoring. Data are presented as mean ± SEM ($n = 11$, $^{***}p < 0.0005$, repeated measures ANOVA). **(B)** Bright field images of sham and contused spinal cords at T10, as indicated by the arrow. ANOVA, analysis of variance; BBB, Basso, Beattie, Bresnahan; SCI, spinal cord injury; SEM, standard error of the mean.

Analysis of N-linked glycosylation

Spinal cord tissue was harvested from animals at 3 and 14 DPI and was either analyzed for the N- and O-linked glycosylation or used for histology. Bright field images of injured spinal cord at T10 show the injury site and confirm the level of injury (Fig. 2B). MALDI-TOF MS and TOF/TOF MS/MS based glycomic methodologies were employed to analyze the N- and O-linked glycosylation from control, sham, 3 DPI, and 14 DPI rat spinal cord samples. Control samples exhibited high mannose (e.g., *m/z* 1579, 1783, 1987, 2192, and 2396), hybrid (e.g., *m/z* 1824, 1998, 2173, and 2203), and complex N-linked glycosylation; the latter ranging from bi- (e.g., *m/z* 2244, 2489, and 2663) to tetra-antennary (e.g., *m/z* 4026, 4213, and 4226) structures and polyLacNAc extended structures (e.g., *m/z* 5023, 5124, and 5485), all mainly core-fucosylated (Supplementary Fig. S1A).

The major non-reducing terminal modification of the complex N-linked glycosylation was sialylation of the antenna LacNAcs Gal-β-(1,4)-GlcNAc, either through the addition of a single NeuAc residue (e.g., *m/z* 4022, 4026, 4400, and 4832) or multiple NeuAc residues (polysialylation, e.g., *m/z* 3514, 3572, 3950, 4063, and 4138) on the same antenna (Fig. 3A and Supplementary Fig. S1A).

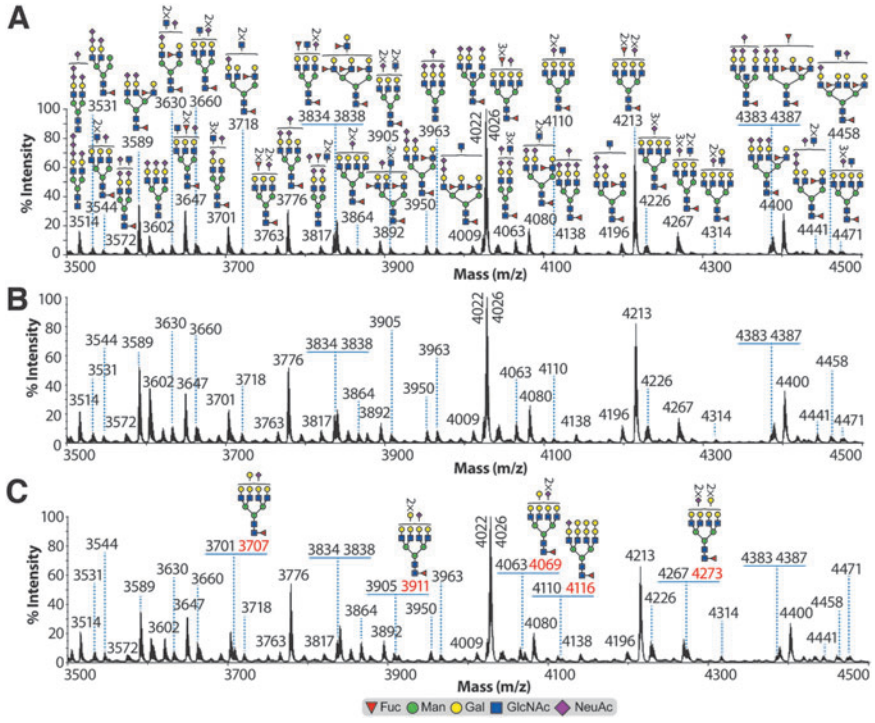

FIG. 3. Partial MALDI-TOF mass spectra of N-linked glycosylation from rat spinal cord samples. Permethylated N-linked glycosylation from **(A)** control, **(B)** sham, and **(C)** 14 DPI samples derived from the 50% acetonitrile fraction (see Methods section). Structures outside a bracket have not been unequivocally defined. Red *m/z* values in (C) 14 DPI correspond to N-linked glycosylation found in increased abundance compared with control and sham samples. Non-annotated *m/z* values in (B) sham and (C) 14 DPI correspond to the same N-linked glycosylation as in the (A) control sample. All molecular ions are $[M+Na]^+$. Putative structures are based on composition, tandem MS, and biosynthetic knowledge. Complete spectra (including 3 DPI) can be found in the supplementary figures (Supplementary Fig. S1). DPI, days post-injury; MALDI-TOF, matrix-assisted laser desorption ionization time-of-flight; MS, mass spectrometry. Color image is available online.

Other additional non-reducing terminal modifications included fucosylation, which formed Lewis^x Gal-β-(1,4)-[Fuc-α-(1,3)]-GlcNAc (e.g., *m/z* 3718, 3838, 3892, 4009, and 4574) structures (Fig. 3A and Supplementary Fig. S1A). Of note is the detection of complex truncated structures (agalactosylated) in the low (e.g., *m/z* 2040, 2081, 2326, 2530, 2646, 2717, 2891, and 3082; Supplementary Fig. S1A) and medium mass range (3544, 3701, 3817, 3892, 4080, and 4267; Fig. 3A). Sham samples exhibited the same N-linked glycosylation structures as the control samples (compare Fig. 3A,B with Supplementary Fig. S1A,B).

Both 3 and 14 DPI injury groups exhibited broadly similar N-linked glycosylation structures as the control and sham samples, but with the following differences. On the 3 DPI samples, complex N-linked glycosylation structures of minor abundances were detected with non-reducing terminal modification corresponding to the Gal-α1,3-Gal structure (e.g., *m/z* 3550, 3619, 3707, 3911, 4069, 4116, and 4273; Supplementary Fig. S1C). These terminal structures were not detected in the control and sham samples. On the 14 DPI samples, most of the above ions were still detected; nonetheless, they appeared to be expressed in lower abundance (Fig. 3C and Supplementary Fig. S1C,D). Interestingly, the ion at *m/z* 3211, which on the control, sham, and 3 DPI samples corresponded to a bi-antennary structure terminated with NeuAc-LacNAcs, on the 14 DPI samples corresponded to a mixture consisting of the latter structure plus a bi-antennary structure with an Sda structure (Neu5Ac-α-(2,3)-[GalNAc-β-(1,4)-]Gal-β-(1,4)-GlcNAc (Supplementary Fig. S1D).

Analysis of O-linked glycosylation

Control and sham O-linked glycosylation (Fig. 4A,B) exhibited core 1 (*m/z* 534) and core 2 (*m/z* 779 and 983) structures terminated with NeuAc residues (*m/z* 895, 1256, 1344, and 1705) or modified with fucose residue forming Lewis^x structures (*m/z* 1157 and 1518). Of note is the presence of a Lewis^x structure and a sialylated structure each attached to an O-mannose type of O-linked glycan (*m/z* 912 and 1099, respectively). SCI (14 DPI) samples (Fig. 4C) exhibited, besides the aforementioned O-linked glycosylation, a striking increase in abundance of core 2 O-linked glycosylation terminated with Sda and Sda-type structures (*m/z* 1794 and 2196; 1140, 1501, and 1589).

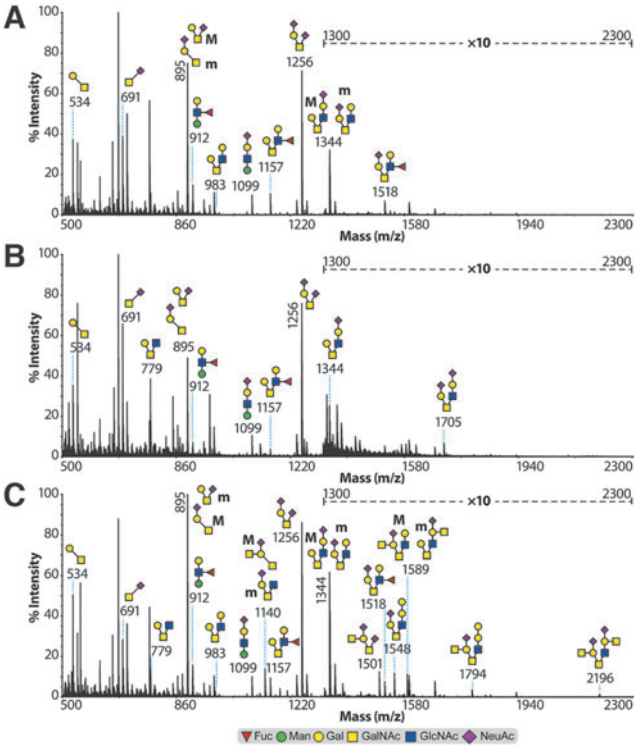

FIG. 4. MALDI-TOF mass spectra of O-linked glycosylation from rat spinal cord samples. Permethylated O-linked glycosylation from **(A)** control, **(B)** sham, and **(C)** 14 DPI samples derived from the 35% acetonitrile fraction (see Methods section). All molecular ions are $[M+Na]^+$. Indicated areas (*m/z* 1300–2300) in the spectra have a 10-fold magnification. Putative structures are based on composition, tandem MS, and biosynthetic knowledge. Full methods and spectra for the 3 DPI samples can be found in the supplementary figures (Supplementary Fig. S4). DPI, days post-injury; MALDI-TOF, matrix-assisted laser desorption ionization time-of-flight; MS, mass spectrometry. Color image is available online.

Sda structure is overexpressed at lesion after SCI

The CT1 antibody binds to the Sda structure with high specificity.[38] Comparison of Sda immunolabeling using CT1 antibody on sham and SCI samples shows an increase of Sda positivity at lesions of SCIs (Fig. 5C). Quantification of Sda fluorescent intensities on shams and SCIs at 14 DPI revealed a significant increase of Sda presence on SCIs (Fig. 5D). On western blot analysis, the Sda exhibited two major bands, one at approximately 67 kD and one at 150 kD (Fig. 5A). Quantification of both bands showed a significant increase in SCI compared with sham at 14 DPI (Fig. 5B). Together, these results indicate a significant increase of Sda at the injured site after SCI.

Microglial cells are main contributors of Sda expression after SCI

To determine which cell types express Sda, we conducted co-immunolabeling of SCI tissue for Sda and various spinal cord cellular markers. Imaging SCI tissue co-labeled for Sda and the microglial marker Iba1 revealed that Sda immunolabeling co-localized to a large extent with Iba1 (Fig. 6A–E). Quantification of mean gray values of Sda and Iba1 at different areas showed both Sda and Iba1 were highest around the injured area (Fig. 6F). These results indicate that Sda intensity mirrors that of microglia, which is highest at the injury site and tapers with distance from the injury site. Not all Iba1 cells stained positive for Sda, and the proportion Sda-negative microglia increased with distance from the injury site.

Expression of Sda on CD8 T lymphocytes and astrocytes

Sda is a blood group structure and previous reports have shown Sda expression on CD8 T cells.[36,39] Because peripheral lymphocytes are known to infiltrate after SCI, tissue was accordingly labeled for CD8 and Sda. Images showed the presence of limited quantities of CD8 T cells in injured spinal tissue, as well as limited Sda labeling of CD8 cells (Supplementary Fig. S2B,D). Sham tissue showed no CD8 T cells (Supplementary Fig. S2A,C). GFAP immunolabeling was also performed and showed that some GFAP cells do label positive for Sda (Supplementary Fig. S3). There were only a small number of GFAP Sda double-positive cells and these tended to be near areas of concentrated Iba1 cells. Triple labeling of GFAP, Iba1,

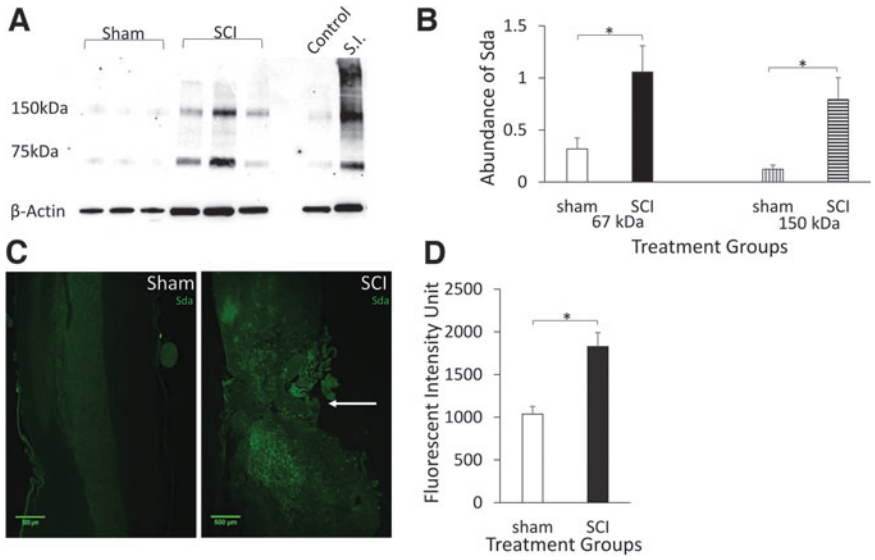

FIG. 5. Expression of Sda structure is upregulated in injured spinal cords. **(A)** Western blot of spinal tissue shows two major bands at 67 kDa and 150 kDa, upregulated in injured spinal cords. Bands on right show control spinal tissue and small intestine (S.I.) positive control. **(B)** Quantification of Sda western blot band intensities. Data are presented as mean + SEM ($n = 5$, $^*p < 0.05$, single-factor ANOVA). **(C)** Fluorescent images of sham and SCI tissue labeled for Sda at T10 (arrow). **(D)** Quantification of Sda fluorescent intensity of sham and SCI at T10. Data are presented as mean + SEM ($n = 6$, $^*p < 0.05$, single-factor ANOVA). ANOVA, analysis of variance; SCI, spinal cord injury; SEM, standard error of the mean. Color image is available online.

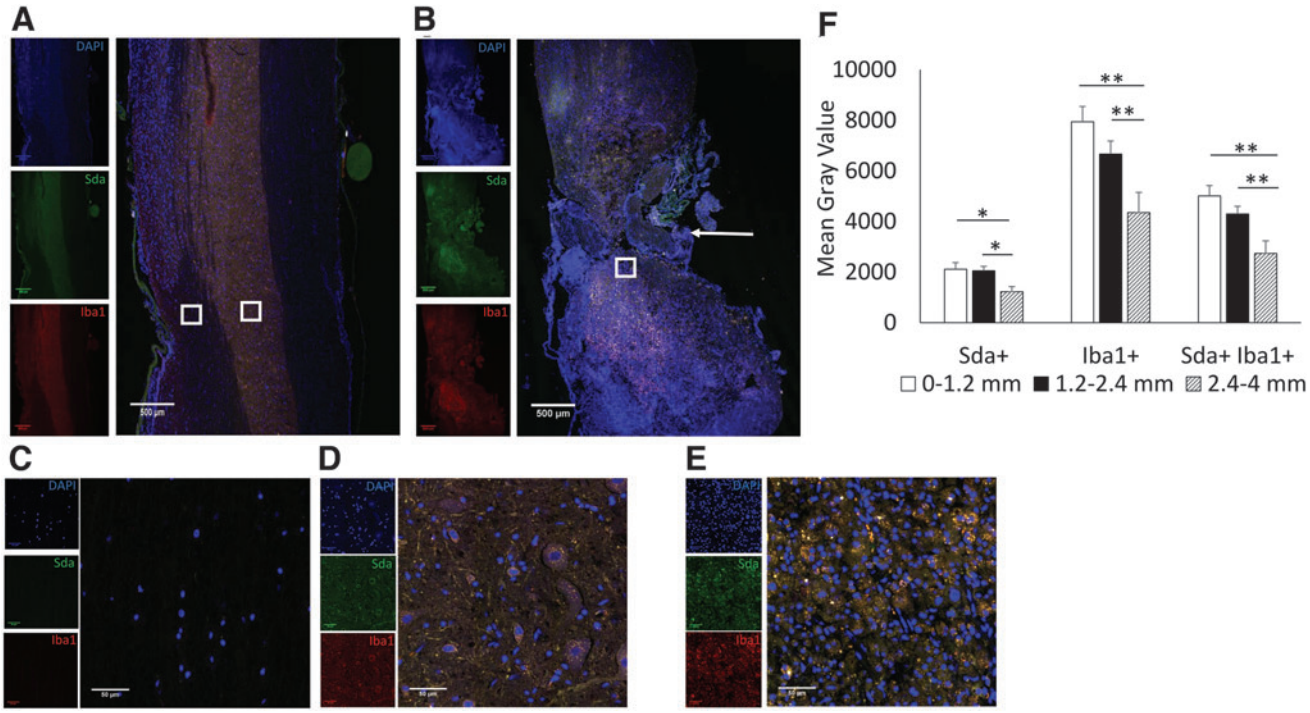

FIG. 6. Co-localization of Sda and Iba1 in injured spinal tissue. Low-magnification images show T10 area from **(A)** sham and **(B)** SCI 14 DPI, indicated by arrow for SCI. **(C)** High-magnification images show white matter from sham. **(D)** High-magnification images show gray matter from sham. **(E)** High-magnification images show boxed area from SCI. Blue (DAPI), green (Sda), red (Iba1). **(F)** Quantification of mean gray values of different distances from injured site for Sda alone, Iba1 alone, and double-positive cells. Data are presented as mean + SEM ($^*p < 0.05$, $^{**}p < 0.01$, single-factor ANOVA). ANOVA, analysis of variance; DAPI, 4',6-diamidino-2-phenylindole; DPI, days post-injury; Iba1, anti-ionized calcium-binding adapter molecule 1; SCI, spinal cord injury; SEM, standard error of the mean. Color image is available online.

and Sda confirmed that some GFAP-positive cells express Sda and it was not an artifact of co-localization of astrocytes and microglia (Supplementary Fig. S5).

Discussion

The balance between growth stimulatory and inhibitory molecules is critical for axonal recovery after SCI. Some carbohydrates, as important components of both growth promoting and inhibiting molecules, are known to play crucial roles in axonal regeneration after SCI.[4] In previous studies, glycosylation structures in the spinal cord, especially the differential glycosylation after SCI, were identified using fluorescent IHC of antibodies and/or lectin histochemistry.[30,40,41] These targeted studies have revealed important glycosylation differences after nervous system injury.

The primary advancement of this study is the identification of N- and O-linked glycosylation structures that are differentially expressed between healthy and injured rat SCI. Results show that the spinal cord has diverse and abundant N- and O-linked glycosylation structures and many individual carbohydrates are differentially expressed with SCI. Both types of glycosylation exhibit a wide range of carbohydrate structures with different abundances (Figs. 3 and 4). The majority of these structures, whether in normal or SCI tissue, are previously undescribed in this context. This underscores the potential impact that a more thorough understanding of glycosylation may have on SCI.

The functional implications of the differentially expressed glycosylation reported here are yet to be determined. However, given that several carbohydrates, such as CSPGs, are already established as playing a significant functional role in SCI, and the sheer diversity of carbohydrate structures described in this study, there is a strong possibility that more carbohydrates with functionally important roles in the injury response and regenerative process exist. Such functional changes in glycosylation should also be considered in the context of potential interactions with carbohydrate-binding proteins. For example, levels of galectin-1 (Gal-1) have been demonstrated to be upregulated in rat spinal cord following standardized contusion injury.[42] Our data show an abundance of multiantennary and polyLacNAc containing N-linked glycans (Fig. 3), which are potential ligands for Gal-1.[43]

However, a limitation of our glycosylation structural analysis is that we have not defined the linkage of the terminal NeuAc residues and it is known that α-2-6-NeuAc, but not α-2-3-NeuAc can inhibit Gal-1 binding.[44] It is not known, however, if Sda impacts Gal-1 binding. Determining the sialic acid linkages would also be important for assessing potential interactions with MAG. MAG is a member of the I-type lectin family and has been demonstrated to have a specificity for NeuAc-α-2,3-Gal, especially on glycolipids such as GD1a and GT1b.[45] MAG has been demonstrated to inhibit axon regeneration following SCI.[46] A continuing challenge is the relative lack of genetic and molecular tools to validate and test the functional importance of an individual carbohydrate or terminal structure.

The Sda structure was one of the significant alterations observed in SCI tissue for which a molecular tool is available. The CT1 antibody, which binds to the Sda structure of Neu5Ac-α-(2,3)-[GalNAc-β-(1,4)-]Gal-β-(1,4)-GlcNAc with high specificity,[38] was an enabling tool to assess the expression of this structure and validate the study. IHC showed that CT1 immunoreactivity increased abundantly in injured spinal tissue and that its expression was primarily associated with microglia at the injury site (Figs. 5 and 6). Interestingly, the abundance of microglia expressing Sda increases with proximity to the injury site (Fig. 6F). CT1 also binds to the GM2 structure, which is identical with Sda for the terminal trisaccharides but has a glucose instead of *N*-acetylglucosamine that links to the rest of the carbohydrate structure.[38] MALDI-MS did not reveal alterations in GM2 in SCI, but it may be possible that CT1 immunoreactivity shown in SCI tissue may have included GM2.

The exact role of Sda and the functional implications of increased Sda on microglia at the injury site are unknown. Sda was first described as a blood group structure and later found to be highly expressed in intestine and several other epithelial tissues.[31,47,48] There are no previous reports that have assessed or observed Sda expression in the CNS, but prior studies suggest roles for Sda in metastasis, rejection of xenotransplants, embryo attachment *in utero*, the development of muscular dystrophy, and CD8-mediated cytotoxicity.[31,38,49–51]

There is some evidence supporting potential mechanisms by which Sda may influence axonal regeneration. The Sda production process competes with synthesis of certain Lewis^x polysaccharides,which are known to promote axonal outgrowth.[52–54] It is therefore possible that the elevated expression of Sda comes at the expense of Lewis^x, potentially impairing regeneration.[24,54] *In vivo* studies with sialidase enzymes, which cleave terminal sialic acids on carbohydrate structures including Sda, among other glycosylation, after SCI promoted recovery.[36,46] Sda on muscle was also shown to bind laminin and agrin at the neuromuscular junction, stabilizing the association between peripheral neurons and muscle cells.[55] Although the exact function of Sda in the spinal cord is unknown, Sda could potentially be affecting axonal outgrowth and synaptogenesis mediated by laminin and agrin.[56,57]

In summary, this study characterized the N- and O-linked glycosylation within the spinal cord in both injured and intact tissue. The data show a diverse array of previously undescribed carbohydrates in spinal tissue and show that significant changes in glycosylation occur as a result of contusion injury. This study was limited in scope to N- and O-linked glycosylation and assessed tissue only at 3 and 14 DPI. Future studies may be warranted to more fully characterize glycomic changes. Such studies would benefit by including analysis of other glycosylation, such as lipid-linked and free carbohydrates, which were not analyzed in the present study, as well as including additional time-points. Given the data of this study, it is likely that additional significant changes in glycosylation occur as a result of SCI.

Acknowledgments

The authors thank Zhaojie Zhang at the University of Wyoming Jenkins Microscopy Facility for assistance with histology and Daniel Burns at the University of Wyoming for assistance with proofreading and editing the manuscript. Content is solely the responsibility of the authors and does not necessarily represent the official views of the funding agencies and sources.

Funding Information

Research reported in this publication was supported by the University of Wyoming Sensory Biology COBRE under the National Institutes of Health (NIH) award number 5P20GM121310-02; by the University of Wyoming Start-up Funds, using equipment funded by the National Institute of General Medical Sciences of the NIH under award number P20GM103432; and by the Biotechnology and Biological Sciences Research Council, grant number BB/K016164/1.

Author Disclosure Statement

No competing financial interests exist.

Supplementary Material

Supplementary Figure S1
Supplementary Figure S2
Supplementary Figure S3
Supplementary Figure S4
Supplementary Figure S5

References

1. Winter, B., Pattani, H., and Temple, E. (2014). Spinal cord injury. Anaesth. Intensive Care Med. 15, 424–427.
2. Sharif-Alhoseini, M., Khormali, M., Rezaei, M., Safdarian, M., Hajighadery, A., Khalatbari, M.M., Safdarian, M., Meknatkhah, S., Rezvan, M., Chalangari, M., Derakhshan, P., and Rahimi-Movaghar, V. (2017). Animal models of spinal cord injury: a systematic review. Spinal Cord 55, 714.
3. Silva, N.A., Sousa, N., Reis, R.L., and Salgado, A.J. (2014). From basics to clinical: a comprehensive review on spinal cord injury. Prog. Neurobiol. 114, 25–57.
4. Ohtake, Y., and Li, S. (2015). Molecular mechanisms of scar-sourced axon growth inhibitors. Brain Res. 1619, 22–35.
5. Jones, L.L., Margolis, R.U., and Tuszynski, M.H. (2003). The chondroitin sulfate proteoglycans neurocan, brevican, phosphacan, and versican are differentially regulated following spinal cord injury. Exp. Neurol. 182, 399–411.
6. Lowe, J.B., and Marth, J.D. (2003). A genetic approach to mammalian glycan function. Annu. Rev. Biochem. 72, 643–691.
7. Zaia, J. (2010). Mass spectrometry and glycomics. OMICS 14, 401–418.
8. Aguiar, C.B.N.M.d., Lobão-Soares, B., Alvarez-Silva, M., and Trentin, A.G. (2005). Glycosaminoglycans modulate C6 glioma cell adhesion to extracellular matrix components and alter cell proliferation and cell migration. BMC Cell Biol. 6, 31–31.
9. Iida, J., Meijne, A.M.L., Knutson, J.R., Furcht, L.T., and McCarthy, J.B. (1996). Cell surface chondroitin sulfate proteoglycans in tumor cell adhesion, motility and invasion. Semin. Cancer Biol. 7, 155–162.
10. Wight, T.N., Kinsella, M.G., and Qwarnström, E.E. (1992). The role of proteoglycans in cell adhesion, migration and proliferation. Curr. Opin. Cell Biol. 4, 793–801.
11. Barone, R., Sturiale, L., Palmigiano, A., Zappia, M., and Garozzo, D. (2012). Glycomics of pediatric and adulthood diseases of the central nervous system. J. Proteomics 75, 5123–5139.
12. Higuero, A.M., Díez-Revuelta, N., Abad-Rodríguez, J.J.H., and Biology, C. (2017). The sugar code in neuronal physiology. Histochem. Cell Biol. 147, 257–267.
13. Kleene, R., and Schachner, M. (2004). Glycans and neural cell interactions. Nature Rev. Neurosci. 5, 195–208.
14. Medina-Cano, D., Ucuncu, E., Nguyen, L.S., Nicouleau, M., Lipecka, J., Bizot, J.-C., Thiel, C., Foulquier, F., Lefort, N., Faivre-Sarrailh, C., Colleaux, L., Guerrera, I.C., and Cantagrel, V. (2018). High N-glycan multiplicity is critical for neuronal adhesion and sensitizes the developing cerebellum to N-glycosylation defect. Elife 7, e38309.
15. Wang, A.C., Jensen, E.H., Rexach, J.E., Vinters, H.V., and Hsieh-Wilson, L.C. (2016). Loss of O-GlcNAc glycosylation in forebrain excitatory neurons induces neurodegeneration. Proc. Natl. Acad. Sci. U S A 113, 15120–15125.
16. Cattaruzza, S., and Perris, R. (2005). Proteoglycan control of cell movement during wound healing and cancer spreading. Matrix Biol. 24, 400–417.
17. Kilcoyne, M., Sharma, S., McDevitt, N., O'Leary, C., Joshi, L., and McMahon, S.S. (2012). Neuronal glycosylation differentials in normal, injured and chondroitinase-treated environments. Biochem. Biophy. Res. Commun. 420, 616–622.
18. Liu, X., Li, A., Ju, Y., Liu, W., Shi, H., Hu, R., Zhou, Z., and Sun, X.J.I. (2018). β4GalT1 mediates PPARγ N-glycosylation to attenuate microglia inflammatory activation. Inflammation 41, 1424–1436.
19. Veillon, L., Fakih, C., Abou-El-Hassan, H., Kobeissy, F., and Mechref, Y. (2018). Glycosylation changes in brain cancer. ACS Chem. Neurosci. 9, 51–72.
20. Bradbury, E.J., Moon, L.D.F., Popat, R.J., King, V.R., Bennett, G.S., Patel, P.N., Fawcett, J.W., and McMahon, S.B. (2002). Chondroitinase ABC promotes functional recovery after spinal cord injury. Nature 416, 636–640.
21. Satoh, J., and Kim, S.U. (1994). Differential expression of Lewisx and sialyl-Lewisx antigens in fetal human neural cells in culture. 37, 466–474.
22. Yaji, S., Manya, H., Nakagawa, N., Takematsu, H., Endo, T., Kannagi, R., Yoshihara, T., Asano, M., and Oka, S. (2014). Major glycan structure underlying expression of the Lewis X epitope in the developing brain is O-mannose-linked glycans on phosphacan/RPTPβ. Glycobiology 25, 376–385.
23. Brito, C., Escrevente, C., Reis, C.A., Lee, V.M.Y., Trojanowski, J.Q., and Costa, J. (2007). Increased levels of fucosyltransferase IX and carbohydrate Lewisx adhesion determinant in human NT2N neurons. J. Neurosci. Res. 85, 1260–1270.
24. Gouveia, R., Schaffer, L., Papp, S., Grammel, N., Kandzia, S., Head, S.R., Kleene, R., Schachner, M., Conradt, H.S., and Costa, J. (2012). Expression of glycogenes in differentiating human NT2N neurons. Downregulation of fucosyltransferase 9 leads to decreased Lewisx levels and impaired neurite outgrowth. Biochim. Biophys. Acta 1820, 2007–2019.
25. Lieberoth, A., Splittstoesser, F., Katagihallimath, N., Jakovcevski, I., Loers, G., Ranscht, B., Karagogeos, D., Schachner, M., and Kleene, R. (2009). Lewis(x) and α2,3-sialyl glycans and their receptors TAG-1, contactin, and L1 mediate CD24-dependent neurite outgrowth. J. Neurosci. 29, 6677.
26. Mehanna, A., Jakovcevski, I., Acar, A., Xiao, M., Loers, G., Rougon, G., Irintchev, A., and Schachner, M. (2010). Polysialic acid glycomimetic promotes functional recovery and plasticity after spinal cord injury in mice. Mol. Ther. 18, 34–43.
27. Pan, H.C., Shen, Y.Q., Loers, G., Jakovcevski, I., and Schachner, M. (2014). Tegaserod, a small compound mimetic of polysialic acid, promotes functional recovery after spinal cord injury in mice. Neuroscience 277, 356–366.
28. Wang, X.-J., Peng, C.-H., Zhang, S., Xu, X.-L., Shu, G.-F., Qi, J., Zhu, Y.-F., Xu, D.-M., Kang, X.-Q., Lu, K.-J., Jin, F.-Y., Yu, R.-S., Ying, X.-Y., You, J., Du, Y.-Z., and Ji, J.-S. (2019). Polysialic-acid-based micelles promote neural regeneration in spinal cord injury therapy. Nano Lett. 19, 829–838.
29. Schnaar, R.L. (2010). Brain gangliosides in axon-myelin stability and axon regeneration. FEBS Lett. 584, 1741–1747.
30. Kilcoyne, M., Patil, V., O'Grady, C., Bradley, C., and McMahon, S.S. (2019). Differential glycosylation expression in injured rat spinal cord treated with immunosuppressive drug cyclosporin-A. ACS Omega 4, 3083–3097.
31. Zhao, C., Cooper, D.K.C., Dai, Y., Hara, H., Cai, Z., and Mou, L. (2018). The Sda and Cad glycan antigens and their glycosyltransferase, β1,4GalNAcT-II, in xenotransplantation. Xenotransplantation 25, e12386.
32. Basso, D.M., Beattie, M.S., and Bresnahan, J.C. (1996). Graded histological and locomotor outcomes after spinal cord contusion using the NYU weight-drop device versus transection. Exp. Neurol. 139, 244–256.
33. Jang-Lee, J., North, S.J., Sutton-Smith, M., Goldberg, D., Panico, M., Morris, H., Haslam, S., and Dell, A. (2006). Glycomic Profiling of cells and tissues by mass spectrometry: fingerprinting and sequencing methodologies, in: *Methods in Enzymology*. Academic Press, pps. 59–86.
34. Ceroni, A., Maass, K., Geyer, H., Geyer, R., Dell, A., and Haslam, S.M. (2008). GlycoWorkbench: a tool for the computer-assisted annotation of mass spectra of glycans. J. Proteome Res. 7, 1650–1659.
35. Belzile, J.-P., Sabalza, M., Craig, M., Clark, E., Morello, C.S., and Spector, D.H. (2015). Trehalose, an mTOR-independent inducer of autophagy, inhibits human cytomegalovirus infection in multiple cell types. J. Virol. 90, 1259–1277.
36. Klisch, K., Jeanrond, E., Pang, P.-C., Pich, A., Schuler, G., Dantzer, V., Kowalewski, M.P., and Dell, A. (2007). A tetraantennary glycan with bisecting N-acetylglucosamine and the Sda antigen is the predominant N-glycan on bovine pregnancy-associated glycoproteins. Glycobiology 18, 42–52.
37. Mountney, A., Zahner, M.R., Sturgill, E.R., Riley, C.J., Aston, J.W., Oudega, M., Schramm, L.P., Hurtado, A., and Schnaar, R.L. (2013). Sialidase, chondroitinase ABC, and combination therapy after spinal cord contusion injury. J. Neurotrauma 30, 181–190.

38. Klisch, K., Contreras, D.A., Sun, X., Brehm, R., Bergmann, M., and Alberio, R. (2011). The Sda/GM2-glycan is a carbohydrate marker of porcine primordial germ cells and of a subpopulation of spermatogonia in cattle, pigs, horses and llama. Reproduction 142, 667.
39. Lefrançois, L., and Bevan, M.J. (1985). Functional modifications of cytotoxic T-lymphocyte T200 glycoprotein recognized by monoclonal antibodies. Nature 314, 449–452.
40. Damjanov, I., and Black, P. (1987). Lectin binding sites on the luminal surface of ependymal cells of the rat spinal cord: implications for neuropathological investigation. Neurosurgery 20, 722–725.
41. Fitch, M.T., and Silver, J. (1997). Activated macrophages and the blood–brain barrier: inflammation after CNS injury leads to increases in putative inhibitory molecules. Exp. Neurol. 148, 587–603.
42. Gaudet, A.D., Sweet, D.R., Polinski, N.K., Guan, Z., and Popovich, P.G. (2015). Galectin-1 in injured rat spinal cord: implications for macrophage phagocytosis and neural repair. Mol. Cell Neurosci. 64, 84–94.
43. Stowell, S.R., Dias-Baruffi, M., Penttilä, L., Renkonen, O., Nyame, A.K., and Cummings, R.D. (2004). Human galectin-1 recognition of poly-N-acetyllactosamine and chimeric polysaccharides. Glycobiology 14, 157–167.
44. Gao, C., Hanes, M.S., Byrd-Leotis, L.A., Wei, M., Jia, N., Kardish, R.J., McKitrick, T.R., Steinhauer, D.A., and Cummings, R.D. (2019). Unique binding specificities of proteins toward isomeric asparagine-linked glycans. Cell Chem. Biol. 26, 535–547.e534.
45. Schnaar, R.L., and Lopez, P.H.H. (2009). Myelin-associated glycoprotein and its axonal receptors. J. neuroscience Res. 87, 3267–3276.
46. Mountney, A., Zahner, M.R., Lorenzini, I., Oudega, M., Schramm, L.P., and Schnaar, R.L. (2010). Sialidase enhances recovery from spinal cord contusion injury. Proc. Natl. Acad. Sci. U S A 107, 11561–11566.
47. Tsubokawa, D., Goso, Y., Kawashima, R., Ota, H., Nakamura, T., Nakamura, K., Sato, N., Kurihara, M., Dohi, T., Kawamura, Y.I., Ichikawa, T., and Ishihara, K. (2012). The monoclonal antibody HCM31 specifically recognises the Sd(a) tetrasaccharide in goblet cell mucin. FEBS Open Bio. 2, 223–233.
48. Kamada, Y., Muramatsu, H., Arita, Y., Yamada, T., and Muramatsu, T. (1991). Structural studies on a binding site for dolichos biflorus agglutinin in the small intestine of the Mouse1. J. Biochem. 109, 178–183.
49. Kawamura, Y.I., Kawashima, R., Fukunaga, R., Hirai, K., Toyama-Sorimachi, N., Tokuhara, M., Shimizu, T., and Dohi, T. (2005). Introduction of Sd(a) carbohydrate antigen in gastrointestinal cancer cells eliminates selectin ligands and inhibits metastasis. Cancer Res. 65, 6220.
50. Nguyen, H.H., Jayasinha, V., Xia, B., Hoyte, K., and Martin, P.T. (2002). Overexpression of the cytotoxic T cell GalNAc transferase in skeletal muscle inhibits muscular dystrophy in mdx mice. Proc. Natl. Acad. Sci. U S A 99, 5616–5621.
51. Lefrancois, L., and Kanagawa, O. (1986). Coordinate expression of cytolytic activity and cytotoxic T cell-specific carbohydrate antigens in a T cell hybridoma. J. Immunol. 136, 1171.
52. Malagolini, N., Santini, D., Chiricolo, M., and Dall'Olio, F. (2007). Biosynthesis and expression of the Sda and sialyl Lewis x antigens in normal and cancer colon. Glycobiology 17, 688–697.
53. Groux-Degroote, S., Wavelet, C., Krzewinski-Recchi, M.-A., Portier, L., Mortuaire, M., Mihalache, A., Trinchera, M., Delannoy, P., Malagolini, N., Chiricolo, M., Dall'Olio, F., and Harduin-Lepers, A. (2014). B4GALNT2 gene expression controls the biosynthesis of Sda and sialyl Lewis X antigens in healthy and cancer human gastrointestinal tract. Int. J. Biochem. Cell Biol. 53, 442–449.
54. Theis, T., Johal, A.S., Kabat, M., Basak, S., and Schachner, M. (2018). Enhanced neuronal survival and neurite outgrowth triggered by novel small organic compounds mimicking the LewisX glycan. Mol. Neurobiol. 55, 8203–8215.
55. Yoon, J.H., Chandrasekharan, K., Xu, R., Glass, M., Singhal, N., and Martin, P.T. (2009). The synaptic CT carbohydrate modulates binding and expression of extracellular matrix proteins in skeletal muscle: partial dependence on utrophin. Mol. Cell Neurosci. 41, 448–463.
56. Freire, E., Gomes, F.C.A., Linden, R., Neto, V.M., and Coelho-Sampaio, T. (2002). Structure of laminin substrate modulates cellular signaling for neuritogenesis. J. Cell Sci. 115, 4867.
57. Daniels, M.P. (2012). The role of agrin in synaptic development, plasticity and signaling in the central nervous system. Neurochem. Int. 61, 848–853.

Address correspondence to:
Jared S. Bushman, PhD
University of Wyoming
1000 East University Avenue, Department 3375
Laramie, WY 82071
USA

E-mail: jbushman@uwyo.edu